Microbial food from light, carbon dioxide and hydrogen gas : kinetic, stoichiometric and nutritional potential of three purple bacteria

MICROBIAL FOOD FROM LIGHT, CARBON DIOXIDE AND HYDROGEN GAS: KINETIC, STOICHIOMETRIC AND NUTRITIONAL POTENTIAL OF THREE PURPLE BACTERIA

Janne Spanoghe[a], Pieter Vermeir[b], Siegfried E. Vlaeminck[a]*

[a] Research Group of Sustainable Energy, Air and Water Technology (DuEL), Department of Bioscience Engineering, University of Antwerp, Groenenborgerlaan 171, 2020 Antwerpen, Belgium

[b] Laboratory for Chemical Analysis, Department of Green Chemistry and Technology, Ghent University, Valentin Vaerwyckweg 1, 9000 Gent, Belgium

*For correspondence. E-mail siegfried.vlaeminck@uantwerpen.be

ABSTRACT

The urgency for a protein transition towards more sustainable solutions is one of the major societal challenges. Microbial protein is one of the alternative routes, in which land- and fossil-free production should be targeted. The photohydrogenotrophic growth of purple bacteria, which builds on the H_2- and CO_2-economy, is unexplored for its microbial protein potential. The three tested species (*Rhodobacter capsulatus*, *Rhodobacter sphaeroides* and *Rhodopseudomonas palustris*) obtained promising growth rates (2.3-2.7 d^{-1} at 28°C) and protein productivities (0.09-0.12 g protein L^{-1} d^{-1}), rendering them likely faster and more productive than microalgae. The achieved protein yields (2.6-2.9 g protein g^{-1} H_2) transcended the ones of aerobic hydrogen oxidizing bacteria. Furthermore, all species provided full dietary protein matches for humans and their fatty acid content was dominated by vaccenic acid (82-86%). Given its kinetic and nutritional performance we recommend to consider *Rhodobacter capsulatus* as a high-potential sustainable source of microbial food.

Keywords: Single-cell protein; Hydrogen economy; Purple non-sulphur bacteria; Photoautotrophy; Essential amino acids

1 INTRODUCTION

The sustainable production of food and feed is one of the major societal challenges of the 21st century. Firstly, the current production chain is severely altering biogeochemical cycles of nitrogen and phosphorus, biodiversity and land-use, with flows towards the biosphere and oceans that are exceeding the planetary boundaries (Campbell *et al.* 2017). Secondly, it is estimated that by 2050, there will be a 50% higher protein demand, with increases up to 82 and 102% for diary and meat products respectively (Boland *et al.* 2013). This illustrates the urgency for a protein transition towards more sustainable solutions to secure the global feed and food supply.

Relevant alternatives are plant-, insect-, and microorganism-based protein products. Microorganisms have among the highest protein content of all organisms, and the use of biomass (e.g. bacteria, algae, yeast and other fungi) for feed or food purposes has been coined 'single cell protein' or 'microbial protein' (MP). Traditionally, the production of MP was predominantly focused on the use of agricultural products or fossil fuels (land- and fossil-based) as electron donors and/or carbon sources (Alloul *et al.* 2021). Pikaar *et al.* (2018) showed that MP produced on sugar cane waste (land- and fossil-based) could lower global crop area use, global nitrogen losses from croplands and agricultural greenhouse gas emissions by respectively 10%, 2% and 1%. However, land- and fossil-free MP production on renewably produced hydrogen gas could lower the pressure even more by 12%, 7% and 9% respectively. This indicated the need to uncouple from agriculture or non-renewable fossil fuels for MP production.

Current routes that are being targeted for land- and fossil-free MP production are (phototrophic) microalgae, aerobic hydrogen oxidizing bacteria, methylotrophs or acetotrophs (Alloul *et al.* 2021). Other appealing microbes for MP production are the purple bacteria (PB). The photoheterotrophic PB have been extensively studied on both production routes, with a focus on wastewater streams, and nutritional quality (Capson-Tojo *et al.* 2020). However, literature on the photoautotrophic growth of PB, all purple non-sulphur bacteria (PNSB), with H_2-gas as electron donor (hydrogenotrophic) is limited and lacks nutritional characterization (Douthit and Pfennig 1976, Madigan and Gest 1979, Colbeau *et al.* 1980, Wang *et al.* 1993, Rey *et al.* 2006). Nevertheless, this metabolism is of high interest as it can be applied on sustainable and renewable resources for energy, electron donor and C/N/P/…, while decoupling from arable land by using:

1. Light energy from the sun or generated via renewable energy
2. Electrons from H_2, from water electrolysis based on renewable energy, syngas from organic waste streams, or from biohydrogen produced by PB photofermentation of organic waste streams (Capson-Tojo *et al.* 2020)
3. Sequestered carbon (carbon capture and utilization), for instance from flue gas or other CO_2-rich exhaust gases
4. Nutrients (N and P), sourced from sustainable production or recovery from waste streams (e.g. $(NH_4)_2SO_4$ and struvite)"

A stoichiometric equation for photohydrogenotrophic PB growth can be derived by balancing electrons, charges and elements (C, H, N and O) assuming (i)

72 photolithoautotrophic growth reducing inorganic carbon with H_2, (ii) ammonium as
73 nitrogen source, (iii) a generic microbial biomass formula ($C_5H_7O_2N$):

$$H_2 + 0.5\ CO_2 + 0.1\ NH_4^+ \xrightarrow{\text{light}} 0.1\ C_5H_7O_2N + 0.8\ H_2O + 0.1\ H^+ \quad \text{Eq. 1}$$

74 Using the expected inorganic carbon equilibrium at pH 7 (28°C) yields:

$$H_2 + 0.10\ CO_2 + 0.40\ HCO_3^- + 0.1\ NH_4^+ + 0.30\ H^+ \xrightarrow{\text{light}} 0.1\ C_5H_7O_2N + 1.20\ H_2O \quad \text{Eq. 2}$$

75 In order to compare the performance of these photohydrogenotrophic PB, microbial
76 protein sources with metabolic similarities are used as a reference point. These are
77 photoautotrophic microalgae, photoheterotrophic PB and hydrogenotrophic hydrogen
78 oxidizing bacteria (HOB).
79
80 It is hypothesized that the metabolic versatility of PB can yield a high tunability of the
81 essential amino acids (EAA), and in extension their nutritional quality, rendering them
82 one of the most attractive MP types (Alloul *et al.* 2021). This tunability was previously
83 seen for photoautotrophic microalgae by species selection or cultivation-based
84 optimization (e.g. nitrogen levels, light intensity and growth phase) (Sui and Vlaeminck
85 2018, Muys *et al.* 2019, Sui *et al.* 2019). Besides the production of protein, PB contain
86 an array of by-products that enrich the nutritional quality further, such as fatty acids,
87 carotenoids, phytohormones and vitamins and promising results were seen already in
88 feeding trials (Capson-Tojo *et al.* 2020).
89
90 In this study, the kinetic and nutritional properties of the photohydrogenotrophic growth
91 for three PNSB were described (*Rhodobacter capsulatus, Rhodobacter sphaeroides* and
92 *Rhodopseudomonas palustris*). The maximum growth rates, biomass productivities,

yields, protein productivities, protein quality (EAA profile), fatty acids and pigment content will be examined through batch cultivation at 28°C. To our knowledge, this paper will be the first determination of all these aspects. Previous literature only briefly discussed maximum growth rates, often only as a subsection of a study. Furthermore, the first verification of dietary protein match for different target organisms (humans, pigs and penaeidae shrimp) will be made, giving insight into the nutritional tunability among the 3 PB species. This study will broaden the knowledge of land- and fossil-free production of PB, providing the foundation for the utilization to its full potential as MP for feed and food.

2 MATERIAL AND METHODS

2.1 SPECIES

Three species were tested in this study of which *Rhodobacter capsulatus (Rh. capsulatus)* was obtained from Alloul *et al.* (2019) whom isolated it from a mixture of activated sludge from a sewage treatment plant, activated sludge from a dairy wastewater treatment plant and sediment from a local pond, after which it was identified by high-throughput 16S rRNA sequencing (Illumina MiSeq; V4 region). *Rhodobacter sphaeroides (Rh. sphaeroides)* (strain: LMG 2827) and *Rhodopseudomonas palustris (Rps. palustris)* (strain: LMG 18881) were ordered from BCCM (Belgian Coordinated Collections of Microorganisms). Originally, all these species were photoheterotrophically enriched from their environments. The three species were stored in aliquots at -80°C and new series of experiments were always started with a fresh aliquot to keep cultures pure, and experiments reproducible.

2.2 GROWTH MEDIUM

The growth medium used was based on Madigan and Gest (1979), yet adapted in the dosage of carbon, nitrogen and phosphorus. Inorganic carbon was dosed as $NaHCO_3$ instead of CO_2 in the gas phase in a concentration of 0.33 g-C L^{-1} (27 mM), while nitrogen was dosed as $(NH_4)_2SO_4$ in a concentration of 0.31 g-N L^{-1} (22 mM). To counteract the consumption of H^+ during photohydrogenotrophic growth, a phosphate buffer system was used. The buffer strength in the medium of Madigan and Gest (1979) was 20 mM, which yielded a fast and high increase in pH that went above pH 8. This had to be avoided to prevent the formation of CO_3^{2-} in the medium. Also, other tested buffers (HEPES and tris) did not control the pH sufficiently within these limits in strengths varying from 10-30 mM. As a result, the monobasic potassium phosphate (KH_2PO_4) was dosed in a concentration of 0.93 g-P L^{-1} (30 mM) which controlled the pH below 8. Nitrogen and phosphorus were thus supplied in excess.

2.3 BATCH GROWTH TESTS

Batch growth tests were performed with Erlenmeyer flasks of 500 mL (DURAN, Germany), with a working volume of 300 mL. At first the autoclavable components of the growth medium were added, after which the bottles were autoclaved at 121°C for 25 minutes. Then the remaining medium components were axenically added after filter sterilization (0.20 µm), while inoculum was added last. The initial biomass concentration was set at an optical density of 0.05 at 660 nm. The Erlenmeyer's were subsequently closed with a gas-tight septum (DURAN, Germany) and the headspace was flushed for 1 minute with a mixture of 80% H_2/20% N_2 at a rate of 1.25 L min^{-1} and set at a gauge pressure of +0.4 bar (absolute pressure 1.4 bar).

139 The Erlenmeyer flasks were constantly mixed on a magnetic stirring plate at 400 rpm
140 (Thermo Scientific, USA) in an incubation chamber (Snijders Scientific, The
141 Netherlands) controlled at 28°C. The light in the incubation chamber was provided by
142 14 fluorescent tubes at a total intensity of 17.9 W m^{-2} (respectively 1.2, 13.8 and 2.8 W
143 m^{-2} in the ranges 175-400, 400-700 and 700-1100 nm). All Erlenmeyer's were
144 randomized daily to provide an even distribution of light. During the experiment the
145 headspace was spiked with 80% H_2/20% N_2 when the gauge pressure dropped below +
146 0.1 bar (absolute pressure 1.1 bar).
147
148 Samples (3 mL) were taken axenically via the gas-tight septum after which the optical
149 density (OD), pH and temperature were measured instantly. The OD at 660 nm was
150 measured with an UV-VIS spectrophotometer (Shimadzu, Japan), while pH and
151 temperature were measured with a handheld device (Hanna Instruments, USA). A
152 maximum of 10 samples (30 mL or 10% of working volume) throughout the experiment
153 was taken to avoid disruption of the growth. After the determination of OD, pH and
154 temperature, samples were frozen (-20°C) for protein, fatty acids and pigments analysis.
155 Gas analysis and headspace pressure were monitored every 24 hours with respectively
156 gas chromatography and a manual manometer. At the end of the batch experiment (t=96
157 hours), samples of the broth were filtered (0.20 µm), to analyze the consumed total
158 ammoniacal nitrogen (NH_3 and NH_4^+) in the medium with a San++Automated Wet
159 Chemistry analyzer (SkalarAnalytical, The Netherlands). Finally, samples (at t=0 and
160 t=96) for molecular analyses are kept at -80°C in case there is an indication of
161 contamination, as is closely monitored by verifying there are no shifts in the optical
162 density spectra during an incubation.

2.4 BIOMASS GROWTH AND PRODUCTIVITY

Bacterial growth (time vs. OD_{660}) was fitted via least squares regression to the Gompertz model modified by Zwietering *et al.* (1990) (time-derivative-type model) in GraphPad Prisma 8 software:

$$\ln\left(\frac{N_t}{N_0}\right) = \ln\left(\frac{N_m}{N_0}\right) * exp\left[-exp\frac{\mu_{max} * e}{\ln\left(\frac{N_m}{N_0}\right)} * (\lambda - t) + 1\right] \quad \text{Eq. 3}$$

in which N_t and N_0 are the biomass concentrations at time t and time 0, N_m is the maximum biomass concentration (reached at stationary phase), μ_{max} is the maximum specific growth rate, λ the lag time, and e the exponential constant (2.718). Maximum growth rates were, if needed, corrected to 28°C, based on an Arrhenius-type of equation assuming a doubling of activity from a temperature increase with 10°C.

The estimated total suspended solids (TSS) levels were based on OD_{660}-TSS correlations that were obtained prior to the detailed growth characterization:

Rh. capsulatus: $\frac{g\ DW}{L} = 433.34 * OD \quad R^2 = 0.94 \quad$ n=12

Rh. sphaeroides: $\frac{g\ DW}{L} = 527.46 * OD \quad R^2 = 0.97 \quad$ n=12

Rps. palustris: $\frac{g\ DW}{L} = 549.81 * OD \quad R^2 = 0.98 \quad$ n=12

The TSS at different well distributed OD values (0.3, 0.6, 1.0 and 1.3) was determined in triplicate via the APHA methods 2540B and 2540D with Whatman® glass microfiber filters by diluting a batch culture at stationary phase. TSS productivities (g TSS L^{-1} d^{-1}) were calculated in two ways, dividing the difference in TSS concentration X (g TSS L^{-1}) relatively to time point zero (overall productivity, t_0, X_0 → t_i, X_i) or between two time points (point-to-point productivity, t_{i-1}, X_{i-1} → t_i, X_i).

2.5 HYDROGEN GAS CONSUMPTION AND DERIVED CALCULATIONS

The percentage of hydrogen gas in the headspace was monitored by gas chromatography (GC-2014) with argon gas as carrier, Shincarbon-ST 50/80 column and TCD detection (shimadzu, Japan). The pressure in the Erlenmeyer flasks was monitored with a manual manometer (Baumer, Germany). Hydrogen gas consumption in the closed system was then calculated with the gas law and the biomass yield (g TSS g^{-1} H_2) was expressed as the net TSS produced to the hydrogen gas consumed.

The availability of dissolved hydrogen gas is an important factor to avoid growth limitation of the purple bacteria. The saturation concentration of dissolved hydrogen gas in the medium is reached when the pressure of the gas above the solution is equal to (i.e. at equilibrium with) the pressure of the gas in the solution. To understand the potential H_2 limitations, dissolved concentrations of hydrogen gas (C_{H2}) were related to microbial growth rates (μ) in the Monod equation (substrate-limiting-type model). This mathematical model could indicate at which dissolved hydrogen concentrations microbial growth would become limited.

Erlenmeyer flasks were set-up in the same manner as the batch growth test with partial pressures of hydrogen (P_{H2}) of 16, 32, 81, 97 and 103 kPa in a total pressure of 141 kPa, which coincidences with dissolved hydrogen concentrations (C_{H2}) of 0.25, 0.50, 1.25, 1.50 and 1.60 mg H_2 L^{-1}. This was done by flushing and spiking the headspace with 80% H_2/20% N_2 and 100% N_2 to reach the appropriate partial pressures. Dissolved hydrogen concentrations were calculated as:

$$C_{H_2} = H * P_{H_2} * MM_{H_2} * 10^3 \ [mg\ H_2\ L^{-1}]$$ Eq. 4

where H is the Henry constant of 7.7 10^{-9} mol L^{-1} Pa^{-1} at 28°C (Fernández-Prini *et al.* 2003), P_{H2} the partial pressure of hydrogen gas in Pa and MM_{H2} the molar mass of hydrogen gas. The saturation concentration (C_{s_H2}) was taken as 1.6 mg H_2 L^{-1}, which was previously found as the maximum solubility in water at 28°C at a P_{H2} of 1 bar (Kolev 2011). Subsequently instantaneous growth rates (point-to-point, based on Gompertz growth model) were plotted against the dissolved H_2 concentration (normalized to atmospheric pressure) at each time point during the experiment. GraphPad Prisma 8 software was used to fit to the Monod model with least squares regression.

Finally, the hydrogen gas utilization rate and the hydrogen gas supply rate were compared to rule out any hydrogen gas limitation during growth. The utilization rate was calculated as:

$$r_{H_2\_demand} = \frac{-\mu * X}{Y_{biomass}} \ [mg\ H_2\ L^{-1}\ d^{-1}]$$ Eq. 5

with μ the growth rate (d^{-1}), X the biomass concentration (mg TSS L^{-1}) and $Y_{biomass}$ the yield (g TSS g^{-1} H_2). The supply rate was determined according to following equation:

$$r_{H_2\_supply} = k_L a * (C_{S\_H2} - C_{H2}) \ [mg\ H_2\ L^{-1}\ d^{-1}]$$ Eq. 6

The volumetric mass transfer coefficient k_La is, among others, proportional to the square root of the diffusion coefficient D (m^2 h^{-1}) of the H_2. Due to the fast-and-easy determination of dissolved oxygen (DO) in the aqueous phase, the k_La for O_2 was determined as a proxy for the k_La of H_2 after which it was converted based on the sole difference in diffusion coefficients in the formula (at 25°C: D_{O2} = 2 x 10^{-5} cm^2 s^{-1}

227 [1]; D_{H2} = 4.5 x 10^{-5} cm^2 s^{-1}). The transfer of H_2 is hence 1.5 times faster

228 than the O_2 transfer.

229

230 The k_La determination was performed in the Erlenmeyer flasks using the same growth

231 medium (section 2.2) and conditions (section 2.3) described earlier, but with two

232 important differences: (i) inoculum was not added to the (abiotic) flasks to avoid biotic

233 oxygen uptake, and (ii) the flaks were kept open to the atmosphere in the incubator to

234 enable the oxygen gas transfer. At the start of the experiment the medium was

235 chemically deoxygenated by adding sodium sulfite and cobalt (Ruchti *et al.* 1985). The

236 DO was measured with an electrode (Hach, USA) until the C_{S_O2} at this temperature

237 was reached. The k_La for oxygen was derived from the slope of the linearization of the

238 DO curve.

239 **2.6 PROTEIN QUANTITY, PRODUCTIVITY AND QUALITY**

240 Protein analysis was performed with a modified Lowry method (Markwell *et al.* 1978).

241 The biomass protein contents were expressed as fractions of the biomass (%TSS).

242 Protein productivities (g protein L^{-1} d^{-1}) were calculated in two ways, dividing the

243 difference in protein concentration (g TSS L^{-1}) relatively to time point zero (overall

244 productivity, t_0, X_0 → t_i, X_i) or between two time points (point-to-point productivity, t_{i-1},

245 X_{i-1} → t_i, X_i).

246

247 Samples for total amino acid (TAA) analysis, and thus also essential amino acids

248 (EAA), were centrifuged (5000×g, 10 min), hydrolyzed (6M HCl, 110 °C, 24 h) with

249 vacuum and evaporated, after which the samples were re-dissolved in 0.75mM HCl and

stored at −20 °C before analysis. Cysteine, methionine and tryptophan could not be quantified with this type of hydrolyzation. The standard operating procedure of Agilent Technologies (Santa Clara, CA, USA) using ortho-phthalaldehyde (OPA)/9-fuorenylmethyl chloroformate (FMOC) derivatization was adopted, with separation using high pressure liquid chromatography and detection using a diode array detector (1290 Infinity II LC System, USA).

As a measure for protein quality, the essential amino acids found in the TAA analysis were used to express the dietary match. The protein quality (g EAA 100 g^{-1} protein) was expressed both on adapted Lowry or TAA protein content and a range of the quality was given:

$$Dietary\ match\ (\%) = \frac{EAA_{product}\left[\frac{g\ EAA}{100\ g\ protein}\right] * digestibility\ (\%)}{EAA_{required\ by\ organism}\left[\frac{g\ EAA}{100\ g\ protein}\right]} \quad \text{Eq. 7}$$

Three target organisms were chosen: humans, pigs and Penaeidae shrimp. As conventional and comparative protein sources meat (beef) (Gorissen and Witard 2018, Kashyap *et al.* 2018), soybean meal and fishmeal were taken (Heuzé V. 2020). The digestibility of the bacterial product was taken as 87.0% (Skrede *et al.* 2009). Furthermore, the essential amino acids index (EAAI) was calculated based on the EAA content in the protein products compared to the EAA requirements (Oser 1959):

$$EAAI = \sqrt[n]{\frac{aa_1}{AA_1} * \frac{aa_2}{AA_2} * \ldots * \frac{aa_n}{AA_n}} \quad \text{Eq. 8}$$

where n is the number of EAA, aa_n and AA_n are the EAA content in the protein product (g EAA g^{-1} protein) and EAA requirement of the organism (g EAA g^{-1} protein) respectively. The quality of the protein is classified according to the EAAI as superior

(>1), high (0.95-1), good (0.86-0.95), useful (0.75-0.86) or inadequate (<0.75) (Kent *et al.* 2015).

2.7 ADDITIONAL NUTRITIONAL PARAMETERS: FATTY ACIDS AND PIGMENTS

Fatty acids (FA) methyl esters were prepared by direct esterification according to a modified procedure (Lepage and Roy 1984) and identified with gas chromatography (Toi *et al.* 2013). The bacteriochlorophyll a (Bchl a) and total carotenoid content were determined by an acetone/methanol solvent (78:22 v/v) extraction, followed by spectrophotometric analysis and conversion with the Lambert-Beer law (Liaaen-Jensen and Jensen 1969, Brotosudarmo *et al.* 2015). Bacteriochlorophyll a has an extinction coefficient of 65.3 mM^{-1} cm^{-1} at a wavelength of 771 nm (Brotosudarmo *et al.* 2015) and a molar mass of 910.5 g/mol. For total carotenoids an average of 97.7 mM^{-1} cm^{-1} is taken as extinction coefficients at the max absorbance between 475 and 525 nm with a molar mass of 596 g/mol based on Liaaen-Jensen and Jensen (1969).

2.8 STATISTICAL ANALYSES

Statistical analyses were conducted in the program 'BM SPSS statistics 26'. One-way ANOVA analyses compared means between objects. The normality of data residuals was tested using the Shapiro-Wilk normality test. The assumption of homoscedasticity was verified through a Levene's test. The Bonferroni post-hoc test was then used to determine significant differences. The non-parametric Kruskal-Wallis rank sum test was executed when normality was rejected. The Welch's t-test was used in case of heteroscedasticity. Repeated measures ANOVA analysis was conducted to analyze differences in results over time (dependent observations). Sphericity (compound

292 symmetry) of the data was tested with the Mauchly's Test and Bonferroni post-hoc
293 analysis gave the final results. A Greenhouse-Geisser correction was done if sphericity
294 was not met.

295 **3 RESULTS AND DISCUSSION**

296 **3.1 GROWTH KINETICS AND PROTEIN PRODUCTIVITY**

297 The growth curves of photohydrogenotrophic PB followed the conventional pattern of
298 lag, log and stationary phase (Figure 1A). With the modified Gompertz model (n=33)
299 maximum growth rates were calculated for *Rh. capsulatus*, *Rh sphaeroides* and *Rps.*
300 *palustris* and were respectively 2.70, 2.30 and 2.33 d^{-1} (corrected to 28°C). A one-way
301 ANOVA confirmed that the μ_{max} of *Rh. capsulatus* was significantly higher (p<0.05)
302 than *Rh. sphaeroides* and *Rps. palustris*. The difference between the latter two was not
303 significant. The difference between the latter two was not significant. It should be noted
304 that the growth stage and activity of the inoculum used (taken from the exponential
305 phase here) may have had a positive impact on the achievable μ_{max}. This is of relevance
306 for the results in section 3.3 below, where a *Rh. capsulatus* inoculum from the late
307 stationary phase yielded a lower μ_{max}.
308
309 Extrapolating and benchmarking growth rates, sometimes obtained under different
310 growth conditions, should be carefully done, yet enables to judge application potential.
311 The maximum growth rates obtained (2.30-2.70 d^{-1}) were in line with
312 photohydrogenotrophic growth rates found in literature, ranging from 0.3 to 3.8 d^{-1} (at
313 28°C) (Douthit and Pfennig 1976, Rey *et al.* 2006), and could hence be higher than
314 microalgal growth rates (0.3-2.4 d^{-1} at 28°C) (Lakaniemi *et al.* 2012, Sunjin Kim 2013,

315 Sui and Vlaeminck 2018, Sui *et al.* 2019). However, compared to photoheterotrophic
316 purple bacteria (0.5-7.2 d^{-1} at 28°C) (Vrati 1984, Willison 1988, Alloul *et al.* 2019) and
317 HOB (1.5-8.8 d^{-1} at 28°C) (Ishizaki and Tanaka 1990, Matassa *et al.* 2016), the μ_{max}
318 obtained under photohydrogenotrophy was in the lower range.
319
320 A repeated measures ANOVA with a Greenhouse-Geisser correction determined that
321 mean protein contents did not differ significantly (p<0.05) along the growth phases
322 (Figure 1C). The average protein content over the whole batch experiment for *Rh.*
323 *capsulatus, Rh. sphaeroides* and *Rps. palustris* were respectively 50.9%, 41.5% and
324 37.9%. These protein contents did differ significantly (p<0.05) with *Rh. capsulatus*
325 achieving the highest protein content. At the end of the batch experiment 74-85 mg N L^{-1}
326 has been consumed from the initially provided N in the medium (310 mg N L^{-1}).
327 Applying the generic protein-to-nitrogen conversion factor of 6.25 on the achieved
328 protein contents in the PB, 50-66% of this N consumption can be attributed to protein
329 production. The remaining N consumption could be attributed to nucleic acid content
330 (typically 30-38% of N in biomass) (Bruce and Perry 2001), Bchl a content (typically
331 0.2-0.5% of N in biomass) or to the possible stripping of NH_3 to the headspace.
332
333 Furthermore, it is seen that the maximal productivities coincides with the early
334 stationary growth phase (Figure 1B). No significant differences (p<0.05) were found in
335 the TSS productivities (overall and point-to-point) over time for a specific species or
336 between species at the same time point. The overall and point-to-point protein
337 productivities shown in Figure 1D correspond with maximum productivities of 0.09-
338 0.12 and 0.16-0.22 g protein L^{-1} d^{-1} and show the same trends as the TSS productivities

339 (Figure 1B). The maximum TSS and protein productivities coincides, as expected, since
340 the protein content does not differ significantly over time. And thus, again, the maximal
341 values are at the start of the stationary phase.
342
343 As previously stated, no nutritional data of photohydrogenotrophically grown PB are
344 available. Therefore, microbial protein sources that express metabolic similarities with
345 the photohydrogenotrophic purple bacteria were selected to enable comparison within
346 the field. Most often, protein productivity is expressed as crude protein in literature,
347 which is the nitrogen content multiplied by a factor 6.25, and results in an
348 overestimation of the total protein content. Therefore protein data measured with the
349 adapted Lowry or TAA method, were converted to crude protein by applying a
350 conversion ratio of 1.31 and 1.33 respectively (Muys *et al.* 2019). Based on the average
351 protein productivities (Figure 2), the photohydrogenotrophic PB in this study are 1.5
352 times faster than microalgae (0.02-0.19 g protein L^{-1} d^{-1}) (Ogbonda *et al.* 2007, Hempel
353 *et al.* 2012, Sui and Vlaeminck 2018), but 4.4 times slower than photoheterotrophic
354 purple bacteria (0.22-0.84 g protein L^{-1} d^{-1}) (Alloul *et al.* 2019, Capson-Tojo *et al.*
355 2020). As expected, the phototrophic protein productivities are well below those of
356 aerobic chemotrophic HOB (1.2-13.1 g protein L^{-1} d^{-1}) (Ishizaki and Tanaka 1990,
357 Matassa *et al.* 2016), due to the difference in energy source (phototrophic versus aerobic
358 hydrogen oxidation) (Schmidt-Rohr 2020)

359 **3.2 H_2-BASED BIOMASS AND PROTEIN YIELDS**

360 The biomass yields in the batch experiment were respectively 5.1, 6.7 and 7.8 g TSS g^{-1}
361 H_2 for *Rh. capsulatus, Rh. sphaeroides and Rps. palustris* at the stationary phase (Figure

362 3A). The expected biomass yield of purple bacteria, based on the stoichiometry (Eq. 2),
363 was 7.0 g TSS g^{-1} H_2. For this, a similar ratio of 0.8 for volatile suspended solids over
364 TSS was used as observed in photoheterotrophically grown PNSB (Alloul *et al.* 2019),
365 with likely phosphorus as important inorganic biomass constituent, not only bound in
366 organic molecules but also stored as polyphosphate (Sakarika *et al.* 2020). Statistical
367 analysis showed that the biomass yield of *Rps. palustris* was significantly higher
368 (p<0.05) than *Rh. capsulatus*, but no significant difference with *Rh. sphaeroides* was
369 found. The protein yield was similarly plotted in Figure 3B and considers the protein
370 content of the three PB species. Contrary to biomass yield, no significant differences
371 were found between species, with values of 2.6, 2.9 and 2.8 g protein g^{-1} H_2. *Rh.*
372 *capsulatus* is able to compensate its lower biomass yield with a significantly higher
373 protein content as seen in Figure 1C.
374 The biomass and protein yields were promising compared to the lower yields of
375 hydrogen oxidizing bacteria, which could be expected based on their stoichiometry
376 (stoichiometry of Matassa *et al.* (2016) was adapted to include biomass as
377 $C_5H_{8.7}O_{2.3}N_{0.9}$):

$$H_2 + 0.3\ O_2 + 0.2\ CO_2 + 0.04\ NH_4^+$$
$$\rightarrow 0.04\ C_5H_{8.7}O_{2.3}N_{0.9} + 0.9\ H_2O + 0.04\ H^+ \qquad \text{Eq. 9}$$

378 resulting in a biomass yield of 2.8 g TSS g^{-1} H_2 (a ratio of 0.8 is assumed for volatile
379 suspended solids over TSS). Actual empirical data for HOB biomass and protein yields
380 found in literature amount to 0.6-2.4 g TSS g^{-1} H_2 and 0.4-1.7 g protein g^{-1} H_2 on
381 average respectively (Ishizaki and Tanaka 1990, Matassa *et al.* 2016). On average, the
382 photohydrogenotrophic PB were thus able to utilize hydrogen gas 3.4 and 2.3 times
383 more efficient for biomass and protein production compared to HOB.

1

3.3 HYDROGEN GAS AVAILABILITY

To rule out any growth limitation due to H_2 availability, a comparison of H_2 supply and uptake rates were made. The Monod relationship (Figure 4A) related the microbial maximum growth rates with the availability of estimated dissolved hydrogen levels. A maximum specific growth rate of 2.12 d^{-1} was found and a half velocity constant K_s of 0.17 mg H_2 L^{-1} (R^2=0.88). The activity of the *Rh. capsulatus* inoculum (late stationary phase) of this series of batch experiments was lower and thus resulted in a lower μ_{max} compared to section 3.1. However, the achieved μ_{max} of *Rh. capsulatus* in section 3.1 was in the same order of magnitude as the two other PB species, which provides confidence in the validity of these results.

Nevertheless, the results still represent a good proxy for limiting hydrogen concentrations. The low value of K_s shows that the growth rate increases rapidly at low aqueous hydrogen gas concentrations. The long-lasting plateau enhances this feature, as still 82% of the maximum growth rate is achieved at half of the saturation concentration of hydrogen gas (0.8 mg H_2 L^{-1}).

Additionally, as gas measurements are time consuming, it was determined whether pressure drop could be used as a proxy for hydrogen gas consumption. The expected pressure drop is calculated by substituting the measured H_2 consumption as follows:

$$\frac{\Delta P}{\Delta m} = \frac{R * T}{MM * V * Vol\%} = 5.04 \qquad \text{Eq. 10}$$

In which it was assumed that the gas composition is fixed (80 vol%-H_2). The nonparametric spearman correlation coefficient between the expected and empirical

405 pressure drops is 0.85. The empirical pressure drop could thus act as a fast proxy for
406 hydrogen gas consumption. The gap between the expected and empirical value can be
407 explained by the gas composition changes. Due to the release of CO_2 to the headspace,
408 via the equilibrium $CO_2/HCO_3^-/CO_3^{2-}$, the volume percentage of H_2 in the headspace is
409 not fixed.

410

411 The mass transfer coefficient of oxygen was determined in the Erlenmeyer flasks and
412 found to be 32.65 d^{-1}. Applying the conversion factor of 1.5, a K_La of 48.97 d^{-1} was
413 found for hydrogen gas. The maximum supply rate of hydrogen gas could then be
414 calculated as 78.36 mg H_2 L^{-1} d^{-1} if the saturation concentration is taken as 1.6 mg H_2 L^{-1}.
415 The hydrogen gas demand rate was plotted for the three PB species in Figure 4B over
416 the course of the batch experiment and showed that no H_2 flux limitation occurred
417 during growth.

418 **3.4 NUTRITIONAL PROFILE: AMINO ACIDS, FATTY ACIDS AND PIGMENTS**

419 The TAA content was quantified at 96 hours in the stationary phase for each species.
420 The applied hydrolyzation on the biomass, destroys the amino acids cysteine,
421 methionine and tryptophan, and thus will result in an underestimation of the TAA.
422 Overall, the *Rhodobacter* species are showing higher TAA content in the TSS, which is
423 similar to what was found with the adapted Lowry method for protein content
424 determination (Figure 1C).

425

426 Compared with the adapted Lowry method, the ratio of Lowry-protein over TAA is
427 1.19, 1.08 and 1.13 for *Rh. capsulatus, Rh. sphaeroides* and *Rps. palustris* respectively.

428 The adapted Lowry method overestimates the total protein content of the PB biomass by
429 an average of 13.5%. However, the adapted Lowry method allows for a fast
430 determination of protein content with a low quantity of sample needed. Furthermore,
431 feed and food industries mostly communicate protein content as crude protein (based on
432 N measurements), which even overestimates the protein content up to 31% (Muys *et al.*
433 2019).
434
435 The content of EAA is more important for the food and feed industry as these cannot be
436 synthesized by our target organisms and must be obtained from feed or food. The nine
437 EAA are: histidine, isoleucine, leucine, lysine, methionine/cysteine,
438 phenylalanine/tyrosine, tryptophan, threonine and valine. The total amount of EAA in
439 the biomass accounts for 37.5, 42.5 and 41.8 % of the TAA for *Rh. capsulatus, Rh.*
440 *sphaeroides* and *Rps. palustris* respectively (Figure 5A). Differences in the profile can
441 be visually distinguished, however, no statistical analysis was performed due to the low
442 number of observations (n=2).
443
444 The dietary match between the three PB species and the human needs was expressed as
445 a min-max range (Figure 5B). The adapted Lowry method often overestimates the true
446 protein content in the biomass, and thus is linked to the minima of the range, while the
447 TAA method, linked to the maxima, gives a slight underestimation, since the applied
448 hydrolysis was unable to quantify three amino acids. It is seen that all PB species are
449 able to fulfill all dietary needs for humans. The dietary match of beef is often the
450 highest, but it is important to note that everything above 100% match will not
451 increasingly add in nutritional quality, as this excess in AA will not be taken up. The

452 dietary match for pigs and penaeidae shrimp have more variable outcomes. However, it
453 is noteworthy that the photohydrogenotrophic PB show a similar protein quality
454 compared to the conventional feed protein sources soybean meal and fishmeal.
455
456 Lastly, Figure 5C shows the EAAI for all target organisms with the PB and
457 conventional protein sources. All EAAI are above 0.75 and thus all PB are adequate
458 candidates as a protein replacement. It is confirmed that all PB species are of superior
459 quality for human food consumption as a protein replacement. Moreover, *Rh.*
460 *capsulatus* showed the highest potential, reaching respectively high and superior protein
461 quality for pigs and penaeidae shrimp according to the EAAI scale (Kent *et al.* 2015).
462 On the other side of the nutritional spectrum, the fatty acid content and composition of
463 each PB is shown in Figure 6. Fatty acids are a major source of energy and can be
464 subdivided in saturated (no double C-C bonds) and unsaturated (mono or poly, which
465 have respectively 1 or more double C-C bonds). Total FA content in the biomass is 6.8,
466 7.1 and 6.1 g FA 100 g^{-1} TSS respectively for *Rh. capsulatus, Rh. sphaeroides* and *Rps.*
467 *palustris.* Microalgae contain FA in the same order of magnitude (7.2 g FA 100 g^{-1}
468 TSS), but with a high composition of saturated fatty acids (39%) (Ortega-Calvo *et al.*
469 1993, Suh *et al.* 2015). Figure 6 shows that the FA profile is dominated by
470 monosaturated FA (91%), with a low amount of saturated FA (7%). The dietary
471 guidelines recommend reducing the intake of saturated fatty acids to reduce the
472 cholesterol levels and thus the risk of cardiovascular disease.
473
474 Interestingly, the results showed high amounts of vaccenic acid (82-86% of total fatty
475 acid content), which is an unambiguous marker of purple bacteria (Imhoff 1991). This is

476 of great importance since vaccenic acid can have a beneficial effect on human health
477 (Field *et al.* 2009). Essential fatty acids, linoleic and α-linolenic, which can be used as
478 precursors to generate a range of fatty acids (Scientific Advisory Committee on
479 Nutrition 2018) were not detected in the three photohydrogenotrophically grown PB.

480

481 Lastly, the main pigments, Bchl a, and carotenoids were determined for *Rh. capsulatus,*
482 *Rh. sphaeroides* and *Rps. palustris*. Both pigments possess antioxidant properties, while
483 carotenoids can decrease the risk of certain cancers and eye diseases for humans
484 (George *et al.* 2020). No significant differences were found between species for both
485 pigments. Bacteriochlorophyll a content in the photohydrogenotrophic PB (0.3-0.6
486 %TSS) was lower compared to levels found in photoheterotrophic PB of 0.7-1.7 %TSS
487 (Alloul *et al.* 2020). Carotenoids, on the other hand, were in the higher range (0.3-0.4
488 %TSS) of values found in literature for photoheterotrophic PB (0.05-0.4 %TSS)
489 (Capson-Tojo *et al.* 2020).

490 **3.5 OUTLOOK**

491 Depending on the chosen source(s) of the sustainable resources (energy, H_2, CO_2,
492 nitrogen, phosphorus,…), the proposed cleantech process can fit in one or more
493 upcoming sustainable economy concepts: the hydrogen economy, the bioeconomy and
494 the circular economy. Microbial food production based on renewable and/or recovered
495 resources with minimal requirement of arable land and fossil-based resources has an
496 excellent environmental sustainability potential. Besides the resource origin options
497 listed in the introduction, an appealing additional option to consider is N_2 as nitrogen
498 source. Purple bacteria are capable of N_2 fixation (George *et al.* 2020), and exploiting

499 this feature could avoid the environmental footprint from synthetic N fertilizer
500 production or from a nitrogen recovery process. The questions to be investigated
501 include the impact of a slightly higher H_2 requirement and hence lower H_2-to-biomass
502 yield, and a potential decrease of the growth rate (and hence protein productivity), both
503 of which were observed previously for HOB (Hu *et al.* 2020).
504
505 Furthermore, the choice of carbon and nitrogen source will also have its effect on the pH
506 control strategy. The stoichiometric equations show the impact of the C species on the
507 pH, with a moderate alkalinization using mainly bicarbonate (–0.3 mol H^+ mol^{-1} H_2) (Eq.
508 2) versus a slight acidification based on CO_2 (+0.1 mol H^+ mol^{-1} H_2) (Eq. 1). Furthermore,
509 using a gaseous N source further affects the balance, with no net pH change
510 stoichiometrically expected based on N_2 dosage:

$$H_2 + 0.43\ CO_2 + 0.04\ N_2 \xrightarrow{\text{light}} 0.09\ C_5H_7O_2N + 0.7\ H_2O \qquad \text{Eq. 11}$$

511 While these assumptions still require experimental validations and additional metabolic
512 pathways may influence the final outcome, pH control based on CO_2 dosage could be an
513 option.
514
515 Looking ahead, a major next research challenge for this concept of microbial food
516 production is intensification in a bioreactor, which will be linked to minimizing H_2 and
517 light limitations, through efficient gas-to-liquid (G-to-L) transfer and supply of light,
518 respectively. Fortunately, both aspects are individually approached in the parallel
519 research, development and innovation activities of two other types of MP or microbial
520 biomass: HOB and microalgae (in closed photobioreactors), respectively. Therefore, the

challenge moves to integrating the 'best of both worlds', and balance the availability of H_2 and light.

HOB production is currently at the stage of industrial validation with microbial products such as Solein, Novomeal and Proton (Alloul *et al.* 2021). Of particular interest here is that the biomass and protein yields of photohydrogenotrophic PB are significantly higher than for HOB, which in combination with their lower growth rates and biomass levels leads to a considerable 142 times lower volumetric H_2 demand rate (Ishizaki and Tanaka 1990, Matassa *et al.* 2016). Therefore, adopting similar G-to-L transfer approaches should be more than sufficient to avoid limitations. Microalgae production in closed photobioreactors is already at the level of industrial demonstration and commercialization with products such as NannoPrime (Proviron) and *Chlorella vulgaris* (Algomed). Insights in optimizing light distribution, proper mixing and the energy need in such photobioreactors can be used (Posten 2009).

4 CONCLUSIONS

Among the photoautotrophs, the three tested species (*Rh. capsulatus*, *Rh. sphaeroides* and *Rps. palustris*) obtained promising growth rates (2.3-2.7 d^{-1} at 28°C) and protein productivities (0.09-0.12 g protein L^{-1} d^{-1}), exhibiting likely faster and more productive characteristics than microalgae. Biomass and protein yields (2.6-2.9 g protein g^{-1} H_2) transcended the ones of aerobic hydrogen oxidizing bacteria by respectively a factor of 3.4 and 2.3, rendering a more resource-friendly MP production. The three species provided a superior protein quality for human dietary needs and vaccenic acid, likely beneficial for humans, was found in high amounts (82-86% of total fatty acid content).

544 E-supplementary data of this work can be found in e-version of this paper online

5 REFERENCES

1 Alloul, A., M. Cerruti, D. Adamczyk, D. G. Weissbrodt and S. E. Vlaeminck (2020). "Control tools to selectively produce purple bacteria for microbial protein in raceway reactors." bioRxiv 912980 [preprint].

2 Alloul, A., J. Spanoghe, D. Machado and S. E. Vlaeminck (2021). "Unlocking the genomic potential of aerobes and phototrophs for the production of nutritious and palatable microbial food without arable land or fossil fuels." Microb Biotechnol.

3 Alloul, A., S. Wuyts, S. Lebeer and S. E. Vlaeminck (2019). "Volatile fatty acids impacting phototrophic growth kinetics of purple bacteria: Paving the way for protein production on fermented wastewater." Water Research **152**: 138-147.

4 Boland, M. J., A. N. Rae, J. M. Vereijken, M. P. M. Meuwissen, A. R. H. Fischer, M. A. J. S. van Boekel, S. M. Rutherfurd, H. Gruppen, P. J. Moughan and W. H. Hendriks (2013). "The future supply of animal-derived protein for human consumption." Trends in Food Science & Technology **29**: 62-73.

5 Brotosudarmo, T. H. P., L. Limantara, Heriyanto and M. N. U. Prihastyanti (2015). "Adaptation of the Photosynthetic Unit of Purple Bacteria to Changes of Light Illumination Intensities." Procedia Chemistry **14**: 414-421.

6 Bruce, E. R. and L. M. Perry (2001). Environmental Biotechnology: Principles and Applications. New York, McGraw-Hill Education.

7 Campbell, B. M., D. J. Beare, E. M. Bennett, J. M. Hall-Spencer, J. S. I. Ingram, F. Jaramillo, R. Ortiz, N. Ramankutty, J. A. Sayer and D. Shindell (2017). "Agriculture production as a major driver of the earth system exceeding planetary boundaries." Ecology and Society **22**.

8 Capson-Tojo, G., D. J. Batstone, M. Grassino, S. E. Vlaeminck, D. Puyol, W. Verstraete, R. Kleerebezem, A. Oehmen, A. Ghimire, I. Pikaar, J. M. Lema and T. Hulsen (2020). "Purple phototrophic bacteria for resource recovery: Challenges and opportunities." Biotechnol Adv: 107567.

9 Colbeau, A., B. C. Kelley and P. M. Vignais (1980). "Hydrogenase Activity in *Rhodopseudomonas capsulata*: Relationship with Nitrogenase Activity." Journal of bacteriology **144**: 141-148.

10 Douthit, H. A. and N. Pfennig (1976). "Isolation and growth rates of Methanol utilizing *Rhodospirillaceae*." Archives of Microbiology **107**: 233-234.

11 Fernández-Prini, R., J. L. Alvarez and A. H. Harvey (2003). "Henry's Constants and Vapor–Liquid Distribution Constants for Gaseous Solutes in H2O and D2O at High Temperatures." Journal of Physical and Chemical Reference Data **32**(2): 903-916.

12 Field, C. J., H. H. Blewett, S. Proctor and D. Vine (2009). "Human health benefits of vaccenic acid." Appl Physiol Nutr Metab **34**(5): 979-991.

13 George, D. M., A. S. Vincent and H. R. Mackey (2020). "An overview of anoxygenic phototrophic bacteria and their applications in environmental biotechnology for sustainable Resource recovery." Biotechnol Rep (Amst) **28**: e00563.

14 Gorissen, S. H. M. and O. C. Witard (2018). "Characterising the muscle anabolic potential of dairy, meat and plant-based protein sources in older adults." Proc Nutr Soc **77**(1): 20-31.

15 Hempel, N., I. Petrick and F. Behrendt (2012). "Biomass productivity and productivity of fatty acids and amino acids of microalgae strains as key characteristics of suitability for biodiesel production." J Appl Phycol **24**(6): 1407-1418.

16 Heuzé V., T. G., Kaushik S.,. (2020, 11/5/2015). "Feedipedia, a programme by INRA, CIRAD, AFZ and FAO.", from https://www.feedipedia.org.

17 Hu, X., F. M. Kerckhof, J. Ghesquiere, K. Bernaerts, P. Boeckx, P. Clauwaert and N. Boon (2020). "Microbial Protein out of Thin Air: Fixation of Nitrogen Gas by an Autotrophic Hydrogen-Oxidizing Bacterial Enrichment." Environ Sci Technol **54**(6): 3609-3617.

18 Imhoff, J. F. (1991). "Polar Lipids and Fatty Acids in the Genus *Rhodobacter*." Systematic and Applied Microbiology **14**(3): 228-234.

19 Ishizaki, A. and K. Tanaka (1990). Batch Culture of *Alcaligenes eutrophus* ATCC 17697 T Using Recycled Gas Closed Circuit Culture System. Journal of fermentation and bioengineering.

20 Kashyap, S., N. Shivakumar, A. Varkey, R. Duraisamy, T. Thomas, T. Preston, S. Devi and A. V. Kurpad (2018). "Ileal digestibility of intrinsically labeled hen's egg and meat protein determined with the dual stable isotope tracer method in Indian adults." Am J Clin Nutr **108**(5): 980-987.

21 Kent, M., H. M. Welladsen, A. Mangott and Y. Li (2015). "Nutritional evaluation of Australian microalgae as potential human health supplements." PLoS One **10**(2): e0118985.

22 Kolev, N. I. (2011). Solubility of O2, N2, H2 and CO2 in water. Multiphase Flow Dynamics 4**:** 209-239.

23 Lakaniemi, A. M., V. M. Intihar, O. H. Tuovinen and J. A. Puhakka (2012). "Growth of *Chlorella vulgaris* and associated bacteria in photobioreactors." Microb Biotechnol **5**(1): 69-78.

24 Lepage, G. and C. C. Roy (1984). "Improved recovery of fatty acid through direct transesterification without prior extraction or purification." Journal of lipid research **25**: 1391-1396.

25 Liaaen-Jensen, S. and A. Jensen (1969). "Quantitative Determination of Carotenoids in Photosynthetic Tissues." **294**: 586-602.

26 Madigan, M. T. and H. Gest (1979). "Growth of the Photosynthetic Bacterium *Rhodopseudomonas capsulata* Chemoautotrophically in Darkness with H2 as the Energy Source." Journal of bacteriology **137**: 524-530.

27 Markwell, M. A. K., S. M. Haas, L. L. Bieber and N. E. Tolbert (1978). "A modification of the Lowry procedure to simplify protein determination in membrane and lipoprotein samples." Analytical Biochemistry **87**(1): 206-210.

28 Matassa, S., W. Verstraete, I. Pikaar and N. Boon (2016). "Autotrophic nitrogen assimilation and carbon capture for microbial protein production by a novel enrichment of hydrogen-oxidizing bacteria." Water Research **101**: 137-146.

29 Muys, M., Y. Sui, B. Schwaiger, C. Lesueur, D. Vandenheuvel, P. Vermeir and S. E. Vlaeminck (2019). "High variability in nutritional value and safety of commercially available Chlorella and Spirulina biomass indicates the need for smart production strategies." Bioresource Technology **275**: 247-257.

30 Ogbonda, K. H., R. E. Aminigo and G. O. Abu (2007). "Influence of temperature and pH on biomass production and protein biosynthesis in a putative Spirulina sp." Bioresource Technology **98**: 2207-2211.

31 Ortega-Calvo, J. J., C. Mazuelos, B. Hermosin and C. Saiz-Jimenez (1993). "Chemical composition of Spirulina and eukaryotic algae food products marketed in Spain." Journal of Applied Phycology **5**: 425-435.

32 Oser, B. L. (1959). An Integrated Essential Amino Acid Index for Predicting the Biological Value of Proteins. Protein and Amino Acid Nutrition. A. A. Albanese. New York, Academic Press**:** 281-295.

33 Pikaar, I., S. Matassa, B. L. Bodirsky, I. Weindl, F. Humpenöder, K. Rabaey, N. Boon, M. Bruschi, Z. Yuan, H. van Zanten, M. Herrero, W. Verstraete and A. Popp (2018). "Decoupling Livestock from Land Use through Industrial Feed Production Pathways." Environmental Science & Technology **52**: 7351-7359.

34 Posten, C. (2009). "Design principles of photo-bioreactors for cultivation of microalgae." Engineering in Life Sciences **9**(3): 165-177.

35 Rey, F. E., Y. Oda and C. S. Harwood (2006). "Regulation of Uptake Hydrogenase and Effects of Hydrogen Utilization on Gene Expression in *Rhodopseudomonas palustris*." Journal of bacteriology **188**: 6143-6152.

36 Ruchti, G., I. J. Dunn and J. R. Bourne (1985). "Practical Guidelines for the Determination of Oxygen Transfer Coefficients (K,a) with the Sulfite Oxidation Method." The Chemical Engineering Journal **30**: 29-38.

37 Sakarika, M., J. Spanoghe, Y. Sui, E. Wambacq, O. Grunert, G. Haesaert, M. Spiller and S. E. Vlaeminck (2020). "Purple non-sulphur bacteria and plant production: benefits for fertilization, stress resistance and the environment." Microb Biotechnol [preprint].

38 Schmidt-Rohr, K. (2020). "Oxygen Is the High-Energy Molecule Powering Complex Multicellular Life: Fundamental Corrections to Traditional Bioenergetics." ACS Omega **5**(5): 2221-2233.

39 Scientific Advisory Committee on Nutrition (2018). Saturated fats and health**:** 233.

40 Skrede, A., L. Mydland and M. Øverland (2009). "Effects of growth substrate and partial removal of nucleic acids in the production of bacterial protein meal on amino acid profile and digestibility in mink." Journal of Animal and Feed Sciences **18**: 689-698.

41 Suh, S.-S., S. J. Kim, J. Hwang, M. Park, T.-K. Lee, E.-J. Kil and S. Lee (2015). "Fatty acid methyl ester profiles and nutritive values of 20 marine microalgae in Korea." Asian Pacific Journal of Tropical Medicine **8**(3): 191-196.

42 Sui, Y., M. Muys, D. B. Van de Waal, S. D'Adamo, P. Vermeir, T. V. Fernandes and S. E. Vlaeminck (2019). "Enhancement of co-production of nutritional protein and carotenoids in *Dunaliella salina* using a two-phase cultivation assisted by nitrogen level and light intensity." Bioresource Technology **287**: 121398.

43 Sui, Y., M. Muys, P. Vermeir, S. D'Adamo and S. E. Vlaeminck (2019). "Light regime and growth phase affect the microalgal production of protein quantity and quality with Dunaliella salina." Bioresource Technology **275**: 145-152.

44 Sui, Y. and S. E. Vlaeminck (2018). "Effects of salinity, pH and growth phase on the protein productivity by *Dunaliella salina*."

45 Sunjin Kim, J.-e. P., Yong-Beom Cho, Sun-Jin Hwang (2013). "Growth rate, organic carbon and nutrient removal rates of Chlorella sorokiniana in autotrophic, heterotrophic and mixotrophic conditions." Bioresour Technol **144**: 8-13.

46 Toi, H. T., P. Boeckx, P. Sorgeloos, P. Bossier and G. Van Stappen (2013). "Bacteria contribute to Artemia nutrition in algae-limited conditions: A laboratory study." Aquaculture **388-391**: 1-7.

730 47 Vrati, S. (1984). "Single cell protein production by photosynthetic bacteria grown
731 on the clarified effluents of biogas plant." Applied Microbiology and Biotechnology
732 **19**(3): 199-202.
733
734 48 Wang, X., H. V. Modak and F. R. Tabita (1993). "Photolithoautotrophic Growth
735 and Control of CO2 Fixation in *Rhodobacter sphaeroides* and *Rhodospirillum rubrum* in
736 the Absence of Ribulose Bisphosphate Carboxylase-Oxygenase." Journal of Bacteriology
737 **175**: 7109-7114.
738
739 49 Willison, J. C. (1988). "Pyruvate and Acetate Metabolism in the Photosynthetic
740 Bacterium *Rhodobacter capsulatus*." Journal of General Microbiology **134**: 2429-2439.
741
742 50 Zwietering, M. H., I. Jongenburger, F. M. Rombouts, K. Van ' and T. Riet (1990).
743 "Modeling of the Bacterial Growth Curve." Applied and environmental microbiology **56**:
744 1875-1881.
745

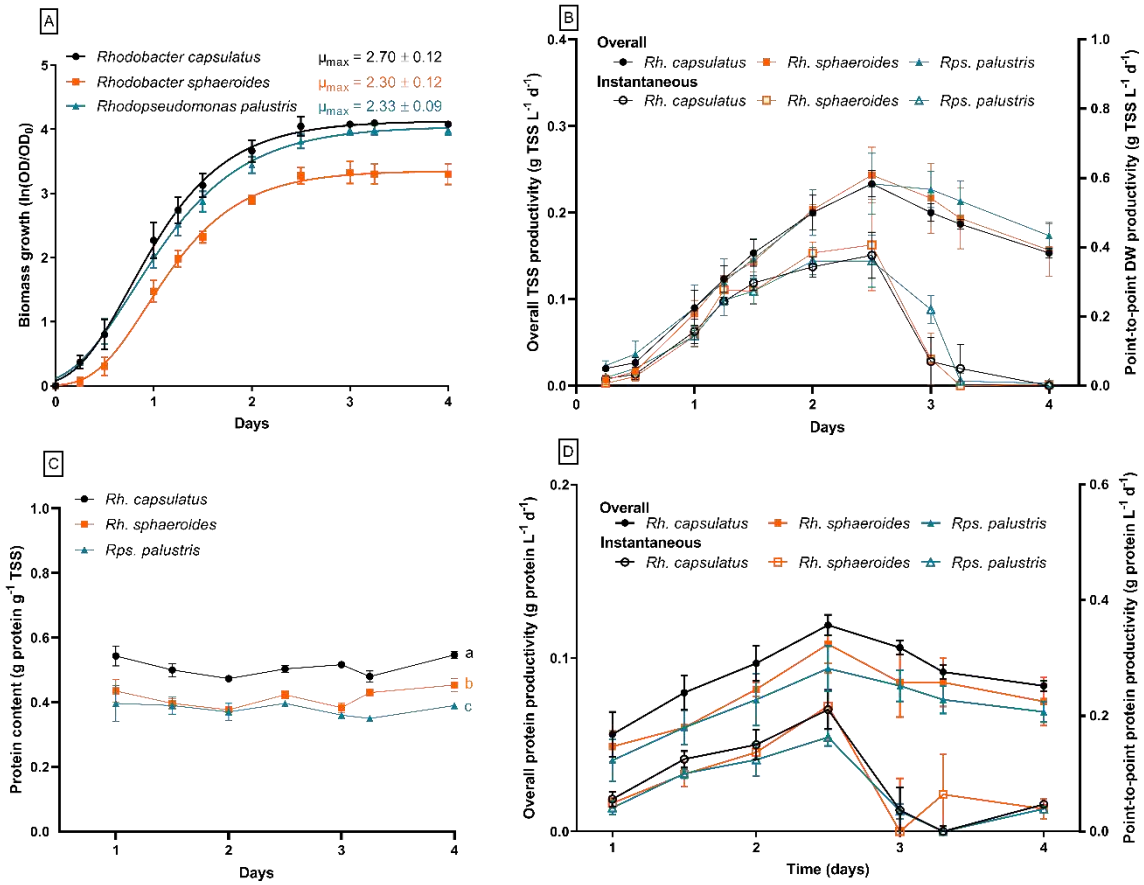

Figure 1: Growth curves of *Rh. capsulatus, Rh sphaeroides* and *Rps. palustris* (panel A) with the modified Gompertz model based on the optical density data over time (n=3 per time point, n=33 for model). Overall and point-to-point total suspended solids (TSS) productivities over the time of the batch experiment (panel B). If the point-to-point productivity was negative, it was set at zero. Each data point shows the average and standard deviation (n=3). Protein content over time for *Rhodobacter capsulatus, Rhodobacter sphaeroides* and *Rhodopseudomonas palustris* (panel C) and overall and point-to-point protein productivities over the time of the batch experiment (panel D). If the point-to-point productivity was negative, it was set at zero. Each data point shows the average and standard deviation (n=3). Letters denote significant differences (p<0.05).

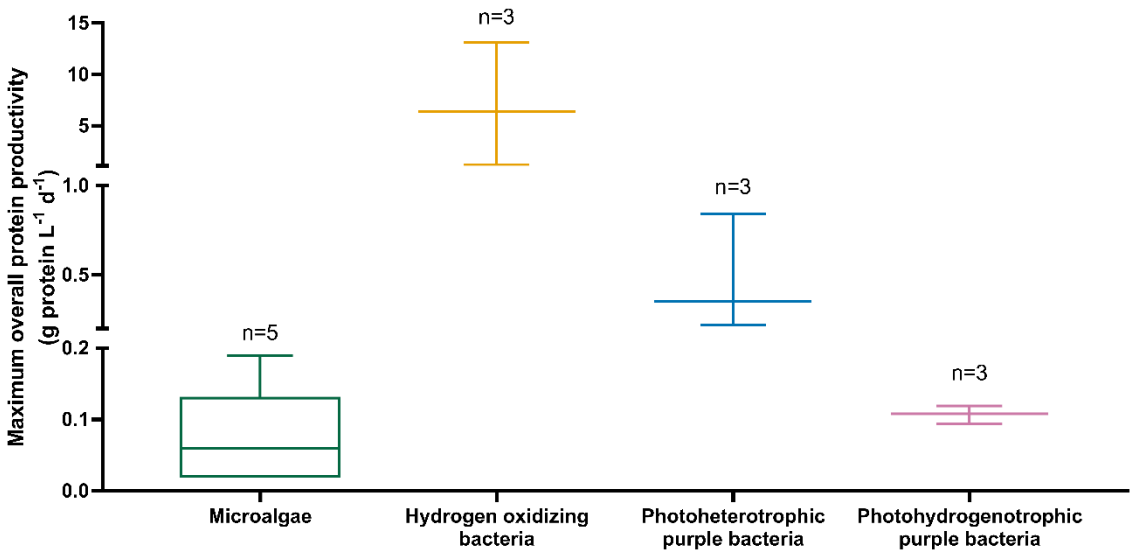

757

758 Figure 2: Comparison between maximum overall protein productivities (often achieved at stationary phase) of
759 microbial protein sources (Ishizaki and Tanaka 1990, Ogbonda *et al.* 2007, Hempel *et al.* 2012, Matassa *et al.* 2016,
760 Sui and Vlaeminck 2018, Alloul *et al.* 2019, Capson-Tojo *et al.* 2020) that express metabolic similarities with
761 photohydrogenotrophic purple bacteria. The maximum protein productivities of photohydrogenotrophic purple
762 bacteria are based on this study. To improve the visibility of the different box plots, the y-axis was divided in 3
763 segments with varying ranges. For each boxplot, the number of observations is given.

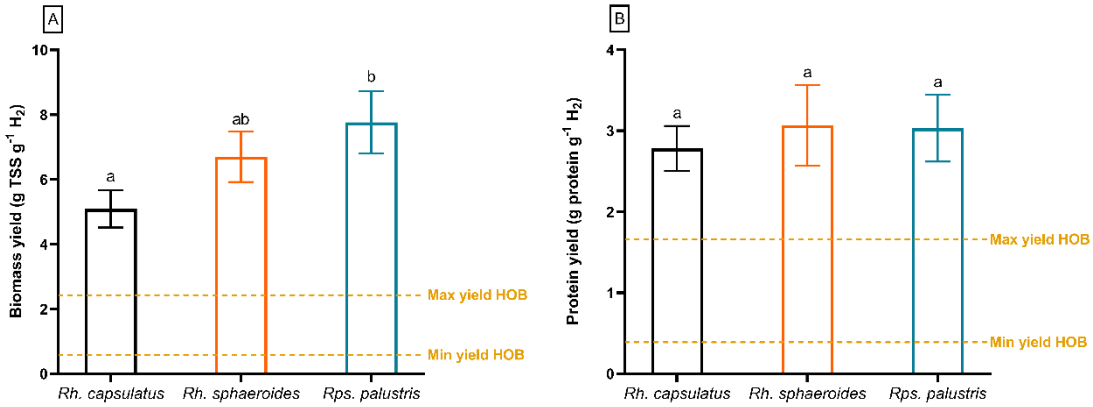

764

765 Figure 3: H_2-based yields of biomass resp. protein production (panel A resp. B) for *Rhodobacter capsulatus,*
766 *Rhodobacter sphaeroides* and *Rhodopseudomonas palustris* at the stationary phase (t=4 days). Average values with
767 standard deviations are given (n=3). Letters denote significant differences (p<0.05). Minimal and maximal empirical
768 yields of hydrogen oxidizing bacteria are given as dashed yellow lines (Ishizaki and Tanaka 1990, Matassa *et al.*
769 2016)
770

3

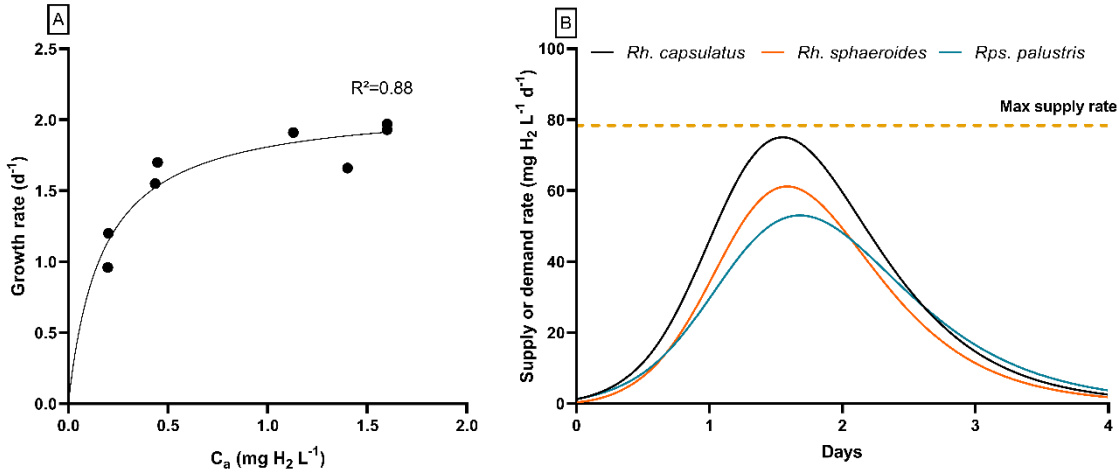

771

772 Figure 4: Hydrogen gas Monod model (panel A) based on the data points found in batch experiments with
773 *Rhodobacter capsulatus* (n=8) at various estimated dissolved H_2 concentrations. Demand rates of hydrogen gas over
774 the course of the batch experiment (panel B) for the three purple bacteria species (full lines) and the maximum
775 supply rate (dashed yellow line).

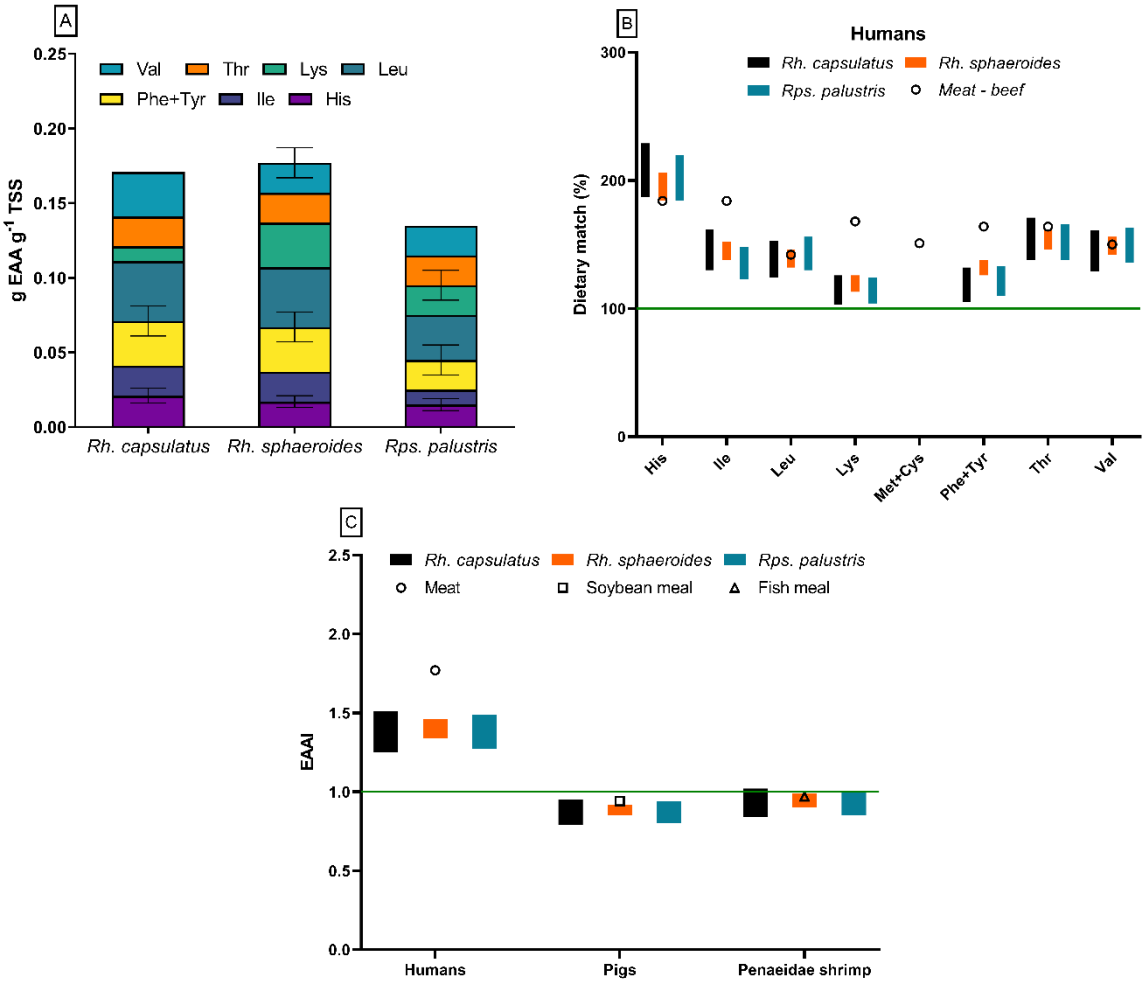

776

777 Figure 5: Essential amino acid (EAA) profile and total EAA content expressed per g of total suspended solids (TSS) for
778 three photohydrogenotrophically grown purple bacteria *(panel A)*; Dietary match between the EAA in the purple
779 bacteria and meat (beef) for humans (panel B); and the essential amino acid index (EAAI) for humans, pigs and
780 Penaeidae shrimp (panel C). Standard deviations are given (n=2), but are omitted from panel B and C to increase
781 visibility of the data.

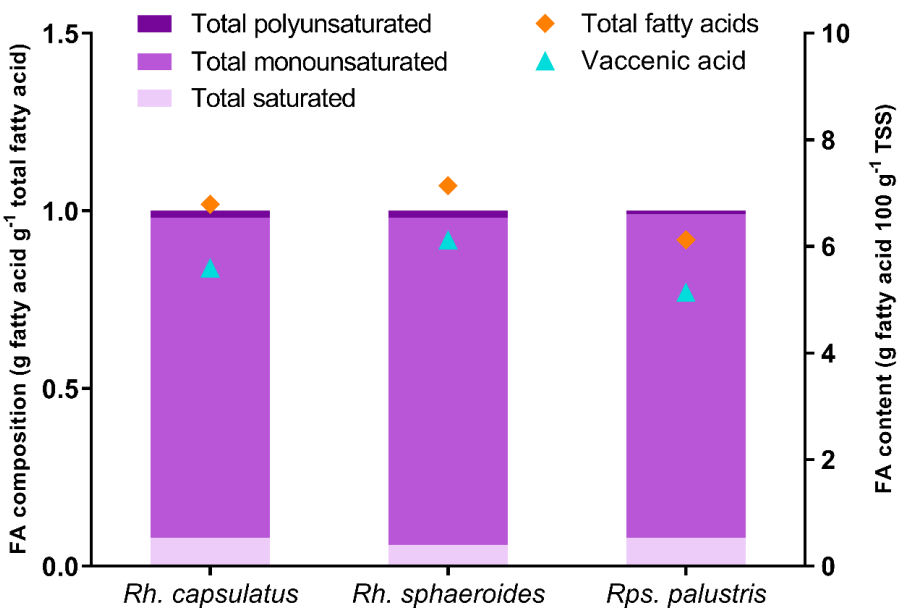

Figure 6: Fatty acid (FA) composition and content in *Rhodobacter capsulatus, Rhodobacter sphaeroides* and *Rhodopseudomonas palustris* at the stationary phase (n=1).